Environmental effects on underwater optical transmission

Peter C. Chu*, Brian F. Breshears, Alexander J. Cullen, Ross F. Hammerer
Ramon P. Martinez, Thai Q. Phung, Tetyana Margolina, Chenwu Fan
Dept. of Oceanography, Naval Postgraduate School, 1 University Circle, Monterey, CA USA 93943

ABSTRACT

Optical communication/detection systems have potential to get around some limitations of current acoustic communications and detection systems especially increased fleet and port security in noisy littoral waters. Identification of environmental effects on underwater optical transmission is the key to the success of using optics for underwater communication and detection. This paper is to answer the question "What are the transfer and correlation functions that relate measurements of hydrographic to optical parameters?" Hydrographic and optical data have been collected from the Naval Oceanographic Office survey ships with the High Intake Defined Excitation (HIDEX) photometer and sea gliders with optical back scattering sensor in various Navy interested areas such as the Arabian Gulf, Gulf of Oman, east Asian marginal seas, and Adriatic Sea. The data include temperature, salinity, bioluminescence, chlorophyll-*a* fluorescence, transmissivity at two different wavelengths (T_{Red} at 670 nm, T_{Blue} at 490 nm), and back scattering coefficient (b_{Red} at 700 nm, b_{Blue} at 470 nm). Transfer and correlation functions between the hydrographic and optical parameters are obtained. Bioluminescence and fluorescence maxima, transmissivity minimum with their corresponding depths, red and blue laser beam peak attenuation coefficients are identified from the optical profiles. Evident correlations are found between the ocean mixed layer depth and the blue and red laser beam peak attenuation coefficients, bioluminescence and fluorescence maxima in the Adriatic Sea, Arabian Gulf, Gulf of Oman, and Philippine Sea. Based on the observational data, an effective algorithm is recommended for solving the radiative transfer equation (RTE) for predicting underwater laser radiance.

Keywords: Radiative transfer equation (RTE), beam attenuation coefficient, absorption coefficient, volume scattering coefficient, scattering phase function, bioluminescence, chlorophyll-*a* fluorescence, HIDEX, SEAGLIDER, EODES

1. INTRODUCTION

For almost a century, the United States Navy has relied on acoustic sensors to map, detect threats or obstacles, and transmit information. However, with limited resources available and the desire to limit exposure to equipment and crew, alternative methods to conduct operations in Anti-submarine Warfare (ASW), Mine Warfare (MIW) and Naval Special Warfare (NSW) are being developed. One such development is the use of electro-optic sensors in conjunction with acoustic sensors to detect, classify, localize and identify sea mines. For example, the AN/AQS-20A Mine Hunting System is a towed body sensor that is operated from naval helicopters. Another sensor deployed in MIW operations is the Airborne Laser Mine Detection System (ALMDS). Increased deployment of autonomous underwater vehicles (AUVs) in a wide range of theaters in support of operations in MIW, fleet survey team (FST), ASW, and NSW has highlighted the limitations in current communications of autonomous systems. AUVs must surface to receive telemetry information and send back data due to the attenuation of radio frequencies in sea water. Two approaches are available for the underwater communication: acoustics using sonar system and optics using light modems to transmit data through water. The advantage of light modem is an unprecedented bandwidth of 1 to 10 megabits per second at up to 200 meters. When combined with acoustic based communications equipment the range can be extended out to much longer ranges[1]. To aid in the deployment and operation of optical sensors in support of Navy operations, the Electro-Optic Detection and Simulation model (EODES) was developed. However, the data input required by the EODES model is not readily available to the sailors in the operational area or as part of a reach-back team. This paper attempts to bridge the gap between readily available data and a high-fidelity performance prediction tool.

*pcchu@nps.edu; phone 1 831 656 3688; fax 1 831 656 3686; http://faculty.nps.edu/pcchu/

Ocean Sensing and Monitoring IX, edited by Weilin (Will) Hou, Robert A. Arnone, Proc. of SPIE
Vol. 10186, 1018609 · © 2017 SPIE · CCC code: 0277-786X/17/$18 · doi: 10.1117/12.2256466

The Naval Oceanographic Office (NAVOCEANO) deployed the High-Intake Defined Excitation Bathyphotometer (HIDEX-BP) into various regional seas with high Navy ‘s interest such as the Yellow Sea, East China Sea, South China Sea, Arabian Gulf, Gulf of Oman, and Adriatic Sea, etc., over more than 10 years on numerous survey ships. Spatial and temporal analysis of the collected HIDEX data will attempt to identify correlations between optical parameters as well as cross correlations between any of the optical parameters with the standard physical parameters sensed in the ocean. From the observed data, various other parameters were derived for studying additional optical and hydrological phenomena that cannot be directly measured by instruments within the current inventory of the naval oceanography community. On the base of the observational results, an effective algorithm to integrate the radiative transfer equation (RTE) for the underwater laser beam propagation for the Navy‘s EODES is also presented.

2. STUDY AREAS

The environmental effects on underwater optical transmission has been determined using the HIDEX data collected by NAVOCEANO survey ships in regional seas with the Navy‘s interests: the Arabian Gulf and Gulf of Oman (Fig. 1a), East China Sea, South China Sea, Yellow Sea, Philippine Sea (Fig. 1b), and Adriatic Sea (Fig. 1c) are selected for study. The Arabian Gulf is connected to the Gulf of Oman through the Strait of Hormuz. The Gulf of Oman opens to the Arabian Sea. The Arabian Gulf is surrounded by Iran, the predominant state in terms of population, and seven Arab states: Iraq, Kuwait, Saudi Arabia, Bahrain, Qatar, the United Arab Emirates and Oman (Fig. 1a). The Yellow Sea is a shallow inland sea that is located between northeastern China and the Korean peninsula. The deepest portion of this body of water is roughly 120 m. The Yellow Sea features a number of large, polluted river outlets including the Yangtze and Yellow Rivers, which serve to add sediment and large particles to the ocean, possibly leading to optical impacts in the measurements obtained [2] [3]. The East China Sea is also a relatively shallow sea that is bounded by mainland China to the west, Japan and the Ryukyu Island Chain to the east, Taiwan to the south, and by the Yellow Sea on its northern border. The most striking bathymetric feature in the East China Sea is the Okinawa Trench, an area of deep water directly to the west of the Ryukyu Island Chain[4]. The South China Sea is a marginal sea of the Pacific Ocean bounded on the north and west by China and Vietnam, to the east by the Philippines and the Luzon Strait, and to the south leads to the maritime continent of Malaysia and Indonesia. The area of data collection is mainly located in the western portion of the South China Sea off the coast of Vietnam in the vicinity of Hainan Island and on the shelf in the northern portion of the South China Sea[5] [6]. The Philippine Sea is composed of a deep abyssal plain bounded by the Ryuku Island Chain to the west and a north-south ridge extending from central Japan down to the Marianas Island Chain to the Marianas Trench[7]. The area directly to the east of Taiwan extends from 4000–5000 meters in depth and is located over an area of highly varied bathymetry (Fig. 1b). The Adriatic Sea is located between the Balkan Peninsula and the Italian Peninsula the Adriatic Sea is the north most basin in the Mediterranean Sea. Its boundaries are set by mountainous terrain to its west, north, and east. The 74 km-wide Strait of Otranto links the Adriatic to the Mediterranean Sea. Rectangular-like in shape, the Adriatic extends 800 km lengthwise and runs from northwest to southeast. On average the width of the Adriatic is 200 km. It is 355 km at its widest and 120 km at its most narrow. The sea can be divided into three major basins. The northern basin gradually slopes towards the southeast reaching a maximum depth of 100 m. It is considered the largest shelf in the Mediterranean and a major source of bottom water formation due to the large volume of river runoff into the shallow basin. The average depth of the basin is 30 m (Fig. 1c).

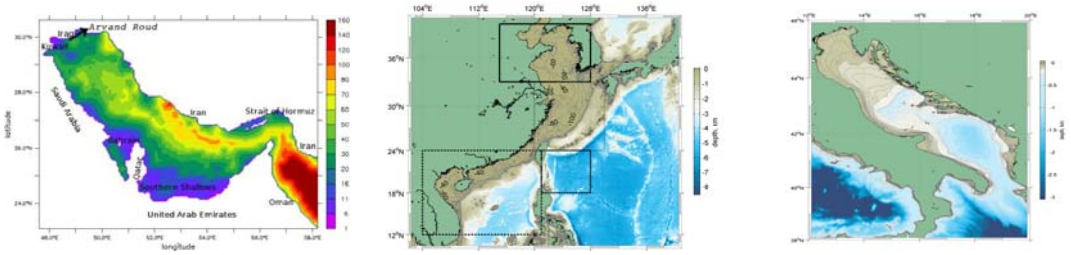

Fig. 1. Study areas (a) Arabian Gulf and Gulf of Oman, (b) East China Sea, Philippine Sea, South China Sea, Yellow Sea, and (c) Adriatic Sea with geographical representation.

3. HIGH-INTAKE DEFINED EXCITATION BATHYPHOTOMETER (HIDEX-BP)

The terminology for describing an instrument that measure vertical distribution of in situ hydrographic parameters (temperature and salinity), inherent optical parameters such as beam attenuation coefficient at near 670 nm (red light) and 490 nm (blue light), bioluminescence, and chlorophyll-a fluorescence (μg/L)[8][9]. For decades, bathyphotometers have been developed in a variety of shapes, sizes and optical configurations. However, the U.S. Navy standard is the High-Intake Defined Excitation Bathyphotometer (HIDEX-BP) (Fig. 2). The vertical resolution of the HIDEX profile data is 1 m. HIDEX was designed and built by the James Case lab at the University of California, Santa Barbara with Navy sponsorship. The HIDEX instrumentation includes the four sensors. A Sea-Bird Electronics (SBE) CTD measures temperature (^{o}C), salinity (psu) and depth (m). A Sea Tech 25 cm path length transmissometer measures red light (~676 nm) transmission (%). To measure chlorophyll-*a* fluorescence (μg/L) at 676 nanometers (nm) wavelength a Chelsea Mk II Aquatracka fluorimeter is used. An Applied Physic Laboratory (APL) 1 meter path length transmissometer measures blue light (490 nm) transmission (%). The HIDEX has a max depth of 200 meters.

HIDEX-BP was delivered to NAVOCEANO in 1990 and has been in continual use ever since, monitoring bioluminescence in the world oceans and adding to the Navy's environmental data base. In 2003, the HIDEX Generation II was developed due to the first generation HIDEX-BP reaching the end of its useful life span. This new design is a fully integrated system that features an improved light collection chamber, new remote telemetry and data acquisitions systems, and most importantly, addition of new sensors to meet expanded measurement requirements. For HIDEX, the topside power supply and computer consoles have been consolidated into two standard 19" mini-racks, each in their own shock-resistant shipping containers[8][9].

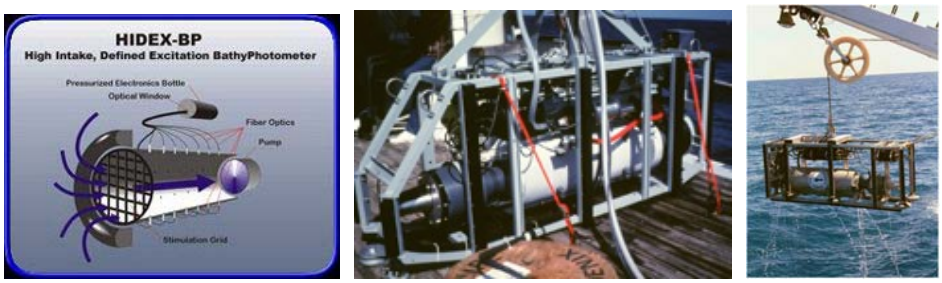

Fig. 2. Illustration of HIDEX-BP observation: (a) light collect chamber, (b) side view, and (c) deployment[8]

The HIDEX data collected by NAVOCEANO for the Arabian Gulf (AG), Gulf of Oman (GO), East China Sea, South China Sea, Yellow Sea, Philippine Sea, and Adriatic Sea are used for this study. Due to the Navy regulation, the tracks of the survey ships cannot be revealed. Table 1 shows the time and location for each survey with HIDEX. Here, the data collection for the Adriatic Sea is taken as an example for illustration. The data was collected from 14 September 2002 to 25 September 2002 as part of a larger Mediterranean cruise. The original data set for the Adriatic included 48 profiles. The cruise started in the North Basin of the Adriatic just outside the Gulf of Trieste and proceeded southeast along a zig-zag pattern. On 23 September 2002, the ship returned north to conduct a series of casts at a single location off the Promontorio del Gargano. After collecting nine profiles over a ten-hour period, the cruise continued southeast. On 25 September 2002, the cruise was concluded.

The HIDEX is a vertical profiler and has an intake flow of up to 35 L/s. Once the water sample is secured in the 1 meter long detection chamber it is agitated to stimulate any bioluminescent organisms that were captured. The large size of the chamber allows for a long residence time to measure the photon flux. This permits a more accurate measurement of the bioluminescent flash that is generated as the total photon flux can be measured compared to an average photon flux that a smaller chamber would measure. Event is measurement used to track the flow rate used during each sample and does not have an associated unit. E fold value is the measure of the first order decay rate and is the time it takes to reach 1/e. Fig. 3 shows an example of HIDEX profile in the Gulf of Oman.

Table 1. Time and location of the HIDEX data collection[10] [11][12]

Month/Year	Survey Location	Number of Profiles	Month/Year	Survey Location	Number of Profiles
JUN 1993	Gulf of Oman	62	MAY 1995	East China Sea	17
JUL 1993	Arabian Gulf	41	JUN 1995	East China Sea	55
MAR 1996	Arabian Gulf	113	APR/MAY 1997	East China Sea	48
APR 1996	Gulf of Oman	46	NOV 1997		35
MAY 2000	Arabian Gulf	46	MAR/APR1998	South China Sea	54
JUN 2000	Arabian Gulf	47	JUL 1999	South China Sea	45
JUN 2000	Gulf of Oman	48	JUN/JUL 2001	Yellow Sea	45
SEP 2000	Gulf of Oman	56	JUN/JUL 2001	Yellow Sea	75
JAN 1995	East China Sea	30	JUN/JUL/AUG 2005	Philippine Sea	28
FEB 1995	Yellow Sea	27	SEP 2012	Adriatic Sea	45
MAY 1995	Yellow Sea	24			

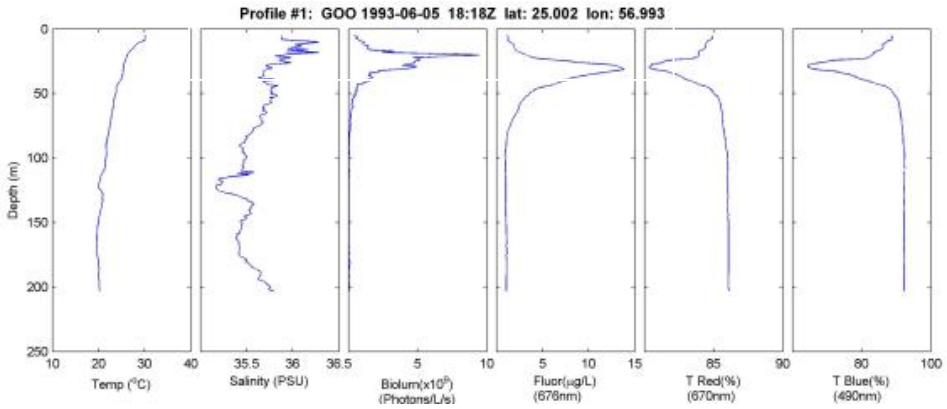

Fig. 3. An example of HIDEX profiles collected in June 1993 in the Gulf of Oman[13]

4. SEAGLIDER

SEAGLIDER is remote operator programmed to perform a series of downward and upward glides while collecting various oceanographic data parameters using variable installed sensor packages [14]. The SEAGLIDER can position itself at the ocean surface with a 45 degree downward angle to present the antenna array skyward to facilitate two way satellite communications. Remote operators can automatically download collected oceanographic data while optionally providing SEAGLIDER with updated mission profile instructions during the pre-programmed sea surface communication periods.
The NAVOCEANO's SEAGLIDER is fitted with the Seabird Electronics SBE 41 CP CTD sensor (hydrographic measurement) and WET Lab s' Environmental Characterization Optics puck, which is comprised of three sensors: a flourometer measuring the bio-optical parameter chlorophyll-a at 470/700 nm wavelengths and two separate and distinct optical sensors measuring the optical backscattering coefficients at the 470 nm and 700 nm wavelengths. The deployed ECO-pucks collected data in the top 300 meters of the water column to preserve battery life and temporally extend the deployment cycles. The flourometer senses chlorophyll-a from 0-30 µg/L and is accurate to within .015 µg/L [15] . Chlorophyll in its various forms is bound within the cells of living organisms. Chlorophyll-*a* is the most abundant form of chlorophyll within photosynthetic organisms. In the ocean water column, the amount of chlorophyll-*a* concentration serves as an indicator of the vertical location of phytoplankton. Chlorophyll fluorescence, when irradiated with light at a particular wavelength, chlorophyll then emits light at a higher wavelength. The seawater is irradiated by the sensor at 470 nm and the chlorophyll-a induced irradiance is then measured at 650-700 nm, and the 470 nm wavelength light is filtered to discount backscatter. The optical backscattering sensors sense from 0 to 5 m^{-1} and are accurate to within 0.003 m^{-1}. The optical backscattering coefficient is measured so that oceanographers can discover various useful factors about

the seawater that has been sampled [16]. Fig. 4 shows an example of a downward-upward cycle of SEAGLIDER profiles collected in October 2010 in the East Asian Marginal Sea.

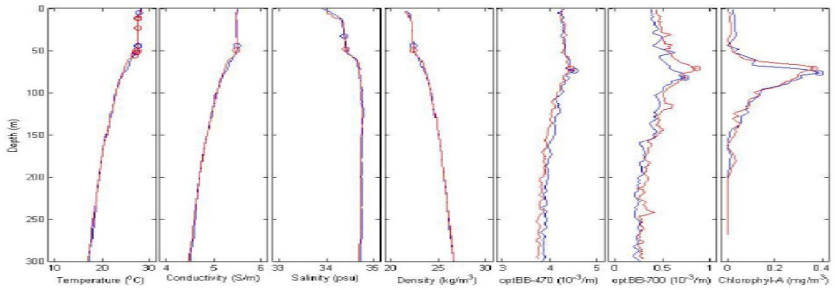

Fig. 4. An example of SEAGLIDER profiles (downward and upward dives) collected in October 2010 in the East Asian Marginal Sea[17].

5. RELATIONSHIP BETWEEN HYDROGRAPHIC AND OPTICAL PARAMETERS

After quality control, cross-correlation coefficients are calculated among the all the parameters at each station and then averaged for all stations for the same survey. Table 2 shows the cross-correlation coefficients in the AG and GO for illustration. Weak cross-correlation coefficients (less than 0.45) are not presented. Here, T is temperature (^{o}C); S is salinity (ppt); B is bioluminescence (phs/s/L); F is fluorescent chlorophyll-a (μg/L), T_{red} is the transmissivity (%) for the red light (670 nm); T_{blue} is the transmissivity (%) for the blue light (490 nm). Strong negative correlation was found between (T, S, B, F) and (T_{red}, T_{blue}) such as -0.71 between T and T_{red} and -0.72 between T and T_{blue} in GO in June 2000, -0.69 between S and T_{red} and -0.72 between S and T_{blue} in GO in September 2000, -0.83 between B and T_{red} and -0.86 between B and T_{blue} in GO in June 2000, -0.85 between F and T_{red} and between F and T_{blue} in the GO in June 2000. Furthermore, T_{red} and T_{blue} are always highly correlated (0.95-0.99). The strong correlation can also be identified from the vertical cross-sections along the observational track of the parameters. Fig. 5 shows such cross sections in the GO in June 2000. The isothermal layer is highly correlated with the isohaline layer. The maximum bioluminescence, fluorescent chlorophyll-a, beam attenuation coefficients (m^{-1}) for red and blue lights were all presented at the base of the mixed layer. Such observational results provide opportunity to link the hydrographic features to underwater optical characteristics.

Evident correlations were also found in other reginal seas such as Adriatic Sea, East China Sea, South China Sea, Yellow Sea, and Philippine Sea. Regression equations were established for each sea,

$$\hat{T}_{red,blue} = \alpha_0 + \alpha_1 T + \alpha_2 S + \alpha_3 B + \alpha_4 F \qquad (1)$$

The regressed transmissivities ($\hat{T}_{red}$, $\hat{T}_{blue}$) are compare to the observed ones, which is given in Fig. 6 for the Adriatic Sea and Fig. 7 for the Philippine Sea. Discrepancy is evaluated by the normalized root mean square errors between $\hat{T}_{red}$ and T_{red}, and $\hat{T}_{blue}$ and T_{blue}, which are the root mean square errors divided by the root mean square of T_{red} or T_{blue}.

Table 2. Mean cross-correlation among hydrographic and optic parameters for the individual survey in AG and GO [12].

		Jun-1993 AG	Jun-1993 GO	Jun-2000 AG	Jun-2000 GO	Mar-1996 AG	Mar-1996 GO	Sep-2000 AG	Sep-2000 GO
T	S	-0.73	0.76	-0.71	0.81	-0.73	0.73	-0.92	0.81
T	B		0.52	0.61	0.73	0.64		0.58	0.46
T	F	-0.55			0.63				0.49
T	T_{red}		-0.68		-0.71		-0.52		-0.67
T	T_{blue}		-0.63		-0.72		-0.56		-0.71
S	B	0.56	0.5	-0.57	0.59			-0.7	0.52
S	F	0.69			0.56			-0.65	0.57
S	T_{red}	-0.68	-0.59		-0.61		-0.54		-0.69
S	T_{blue}	-0.62	-0.57		-0.61		-0.58		-0.72
B	F	0.57	0.71		0.73		0.73	0.56	0.74
B	T_{red}		-0.8		-0.83		-0.75	-0.5	-0.75
B	T_{blue}		-0.82		-0.86		-0.73	-0.54	-0.75
F	T_{red}	-0.68	-0.82		-0.85		-0.79	-0.61	-0.79
F	T_{blue}	-0.66	-0.82		-0.85		-0.77		-0.78
T_{red}	T_{blue}	0.95	0.98	0.95	0.99	0.96	0.97	0.97	0.98

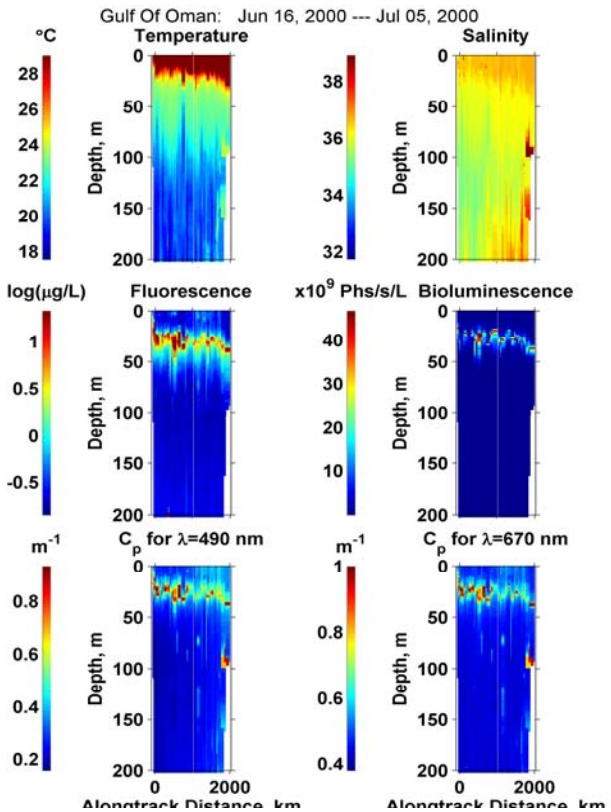

Fig. 5. Along track vertical cross-sections of temperature, salinity, bioluminescence, fluorescent chlorophyll-a, beam attenuation coefficients (m^{-1}) for red and blue lights in the Gulf of Oman from 16 June to 5 July 2000 [12].

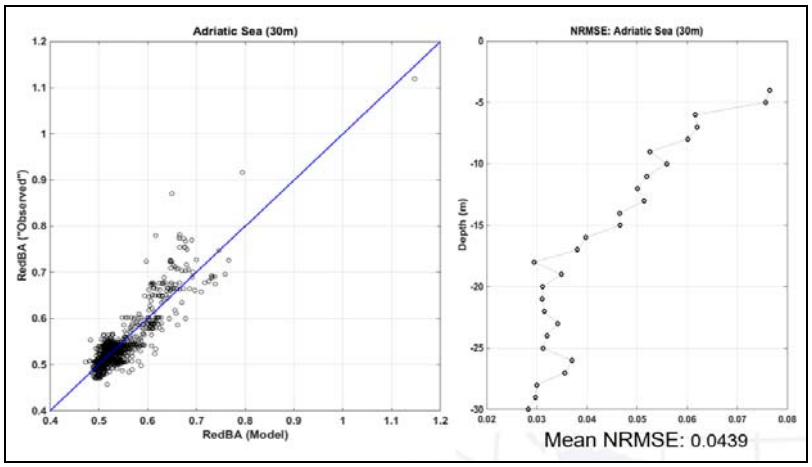

Fig. 6. Comparison between regresses and observed transmissivity of the red light (670 nm) in the Adriatic Sea with the normalized root mean square error of 0.0439 [10].

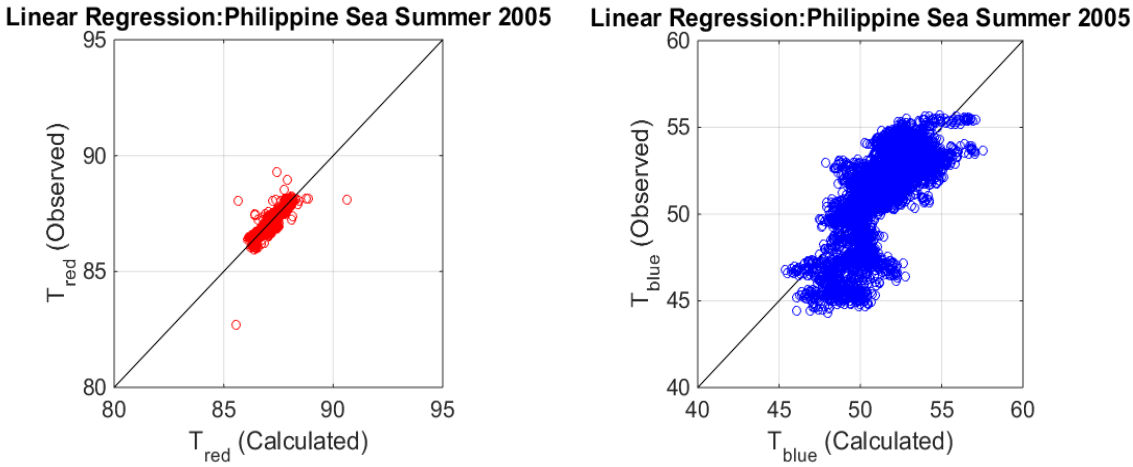

Fig. 7. Comparison between regresses and observed transmissivity of the (a) red light (670 nm) and (b) blue light (490 nm) in the Philippine Sea with the normalized root mean square error is 0.0013 for T_{red} and 0.0331 for T_{blue} [11].

6. TWO TYPES OF SIMPLIFICATION ON SCATTERING PHASE FUNCTION

Let $\mathbf{r} = (x, y, z) = (r, \phi, \theta)$ be the position vector with z in vertical and (x, y) in horizontal; and $\mathbf{s} = (\xi, \eta, \zeta) = (\vartheta, \varphi)$ with $|\mathbf{s}|=1$ be the direction vector (Fig. 8a). The radiative transfer equation for a given light frequency under small angle assumption is given by

$$\left[\cos\vartheta\frac{\partial}{\partial z} + \mathbf{s}\bullet\nabla + c(z)\right]L(\mathbf{r},\mathbf{s}) = b(z)\int_{2\pi}\beta(\mathbf{s},\mathbf{s}')L(\mathbf{r},\mathbf{s}')\frac{d\xi'}{\cos\vartheta} + B(\mathbf{r},\mathbf{s}) \qquad (2)$$

where $L(\mathbf{r}, \mathbf{s})$ is the radiance [Watts/(m^{2}sr)]; Ω is the solid angle; $\beta(\mathbf{s},\mathbf{s}')$ is the scattering phase function with $\mathbf{s}'$ the original direction of the photon flux and $\mathbf{s}$ the direction after deflection by scattering; c(z) and b(z) are the depth-dependent beam attenuation and volume scattering coefficients, and $B(\mathbf{r}, \mathbf{s})$ is the source term such as the bioluminescence. The ratio, $\omega = b / c$, is defined as the single scattering albedo with the typical value between 0.7 and 0.8 [18]. Among them, only $c(z)$ [or $b(z) = \omega c(z)$], and $B(z)$ [i.e., horizontally and directionally averaged] are measured from the NAVOCEANO ships. The scattering phase function $\beta(\mathbf{s},\mathbf{s}')$ is hard to observe and usually to get under special conditions.

6.1. Axisymmetric scattering

With the axisymmetric scattering, the scattering phase function $\beta(\mathbf{s},\mathbf{s}')$ is given by

$$\beta(\mathbf{s},\mathbf{s}') = \hat{\beta}(|\xi - \xi'|) \qquad (3)$$

where $\xi = (\zeta, \eta)$; $\hat{\beta}(|\xi - \xi'|)$ is the axisymmetric scattering phase function with ξ' the original direction of the photon flux and ξ the direction after deflection by scattering $\hat{\beta}(\alpha)$ is taken as given functions for different types of scattering. The Navy's EODES model[18] is to solve the radiative transport equation (RTE) with no forcing term under axisymmetric scattering in wavenumber space,

$$\left[\frac{\partial}{\partial z} - i\xi\bullet\mathbf{k} + c(z)\right]L(z,\mathbf{k},\xi) = b(z)\int_{2z}\beta(|\xi - \xi'|)L(z,\mathbf{k},\xi')d\xi' \qquad (4)$$

where $\mathbf{k} = (k_x, k_y)$ is the Fourier conjugate spatial variable; $i = \sqrt{-1}$; $L(z,\mathbf{k},\xi)$ is the spatial Fourier transform of the radiance [Watts/(m^{2}sr)]; is the direction vector.

6.2. Azimuthally symmetric scattering and absorption

With the azimuthally symmetric scattering and absorption, the radiance for any azimuth angle on the same circle is the same (Fig. 8b). Thus, the position vector, $\mathbf{r} = (x, \rho)$, and the direction vector $\mathbf{n}$ depending on ϕ are two dimensional. The RTE is two dimensional,

$$\mathbf{n}\bullet\nabla L(\rho, z, \mathbf{n}) = -cL(\rho, z, \mathbf{n}) + b\int_{2\pi} \beta(\mathbf{n}, \mathbf{n}')L(\rho, z, \mathbf{n}')d\mathbf{n}' + B(\rho, z, \mathbf{n}) \qquad (5)$$

If the 2D Henyey-Greenstein (H-G) phase function is used for the azimuthally symmetric scattering,

$$\beta(\mathbf{n}, \mathbf{n}') = \frac{1 - g^2}{2\pi(1 + g^2 - 2g\cos\theta)} \qquad (6)$$

where θ is the scattering angle between $\mathbf{n}$ and $\mathbf{n}'$, i.e., $\mathbf{n}\bullet\mathbf{n}' = \cos\theta$; g is the asymmetry parameter (ranging from 0 to 1) with $g = 0$ for dominating isotropic scattering and g near 1 for peaked scattering. As a strong forward scattering medium, the sea water's g varies between 0.8 and 0.95 [19], which is potentially beneficial for underwater optical communication. The position and direction vectors are discretized by (ρ_i, z_j, θ_k) with increments $(\Delta\rho, \Delta z, \Delta\theta)$, the differential-integral RTE becomes linear algebraic equation [20],

$$\sin\theta_k \frac{L_{k,i,j} - L_{k,i-1,j}}{\Delta\rho} + \cos\theta_k \frac{L_{k,i,j} - L_{k,i,j-1}}{\Delta z} + c_j L_{k,i,j} = b_j \sum_{k'=1}^{K} p_{k,k'} L_{k',i,j} + B_{k,i,j}, \quad b_j = \omega c_j \qquad (7)$$

where $p_{k,k'}$ is the discretized phase function (6); K is the total number of the angle sections. The Gauss-Seidel iteration ([20] Lie et al. (2015) is used to solve the algebraic equation (7) using the observed beam attenuation coefficient (c_j).

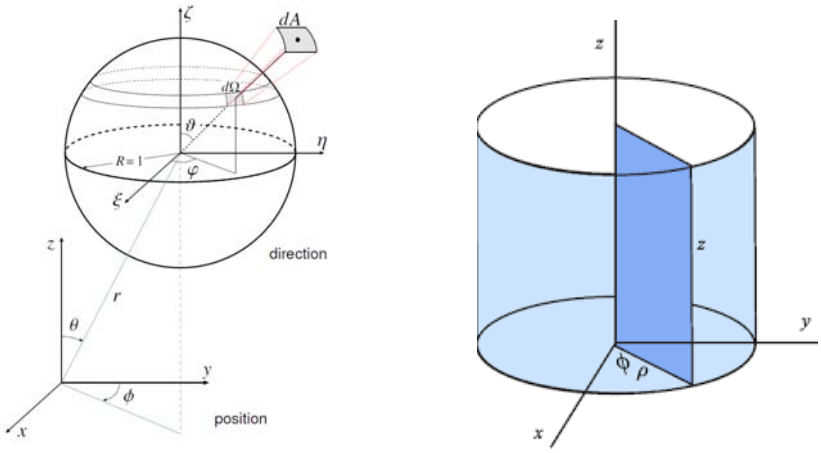

Fig. 8. Position and direction coordinates (a) with axisymmetric scattering (from Giddings and Shirron 2011) and (b) with azimuthal symmetric scattering and absorption.

7. NUMERICAL SOLUTIONS

The single scattering albedo is selected as its averaged value for the East Asian Marginal Seas, $\omega = 0.75$. The laser is treated as a point source located at the ocean surface. The back scattering coefficient (b_j) measured from the NAVOCEANO's SEAGLIDER is used to calculate the beam attenuation coefficient (c_j). The discretized RTE (7) is integrated numerically using two distinct optical profiles collected from the SEAGLIDER: large beam attenuation coefficient (Fig. 9a) and small beam attenuation coefficient (Fig. 9b). The simulated laser beam penetrates much deeper with small beam attenuation coefficient than with large beam attenuation coefficient. With the developed numerical algorithms to solve underwater RTE and statistical analysis between environmental and optical parameters, a coupled ocean circulation and underwater RTE model may be developed with a new statistical module as a key component linking environmental parameters (e.g., temperature, salinity, chlorophyll-*a*) to underwater optical parameters (e.g.,

beam attenuation coefficient). Fig. 10 shows the flow chart of such a system. Both modeled (from the statistical module) and observed beam attenuation coefficients will be assimilated into the Navy's EODES for tactical decision aid for Navy operations.

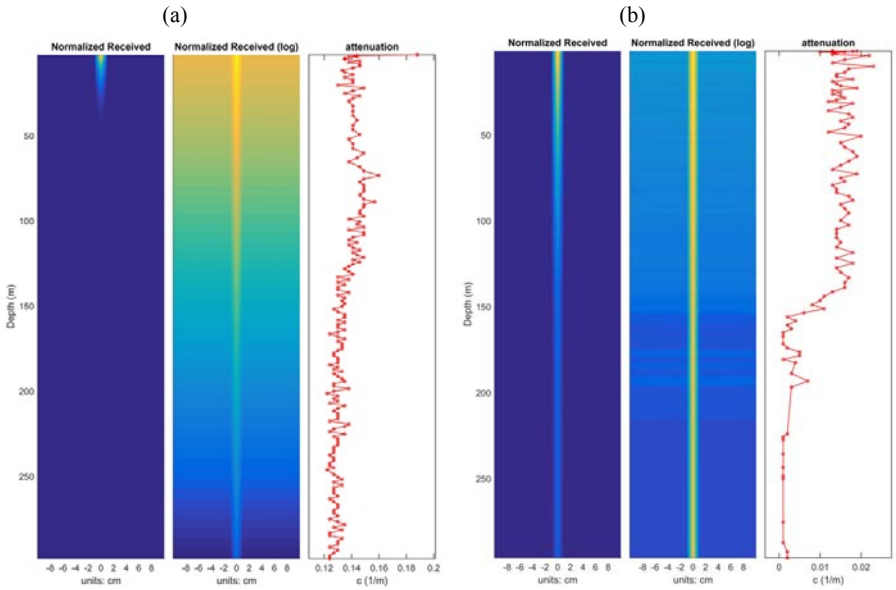

Fig. 9. Normalized radiance $L(\rho, z)$ simulated using Eq.(7) with the beam attenuation coefficients obtained from the NAVOCEANO 's SEAGLIDER: (a) large and (b) small beam attenuation coefficients. Here, middle panel of each figure is $L(\rho, z)$ in log scale.

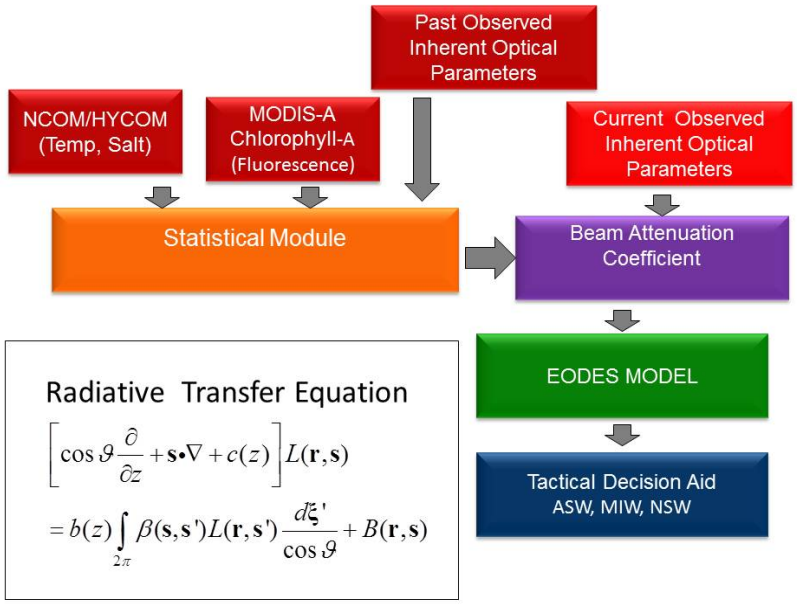

Fig. 10. Flow chart of near future Electro-Optic Detection and Simulation with assimilating ocean numerical modeled and satellite observed data.

8. CONCLUSIONS

This study identifies the ocean environmental effects on underwater optical transmission in several regional seas such as the Arabian Gulf, Gulf of Oman, East China Sea, South China Sea, Yellow Sea, Philippine Sea, and Adriatic Sea using the data collected by NAVOCEANO from survey ships with HIDEX and SEAGLIDERs and the Navy's EODES model. Statistical analysis on the HIDEX and SEAGLIDER data shows strong negative correlation between (chlorophyll-*a* fluorescence, temperature, salinity) and transmissivity (or strong positive correlation to beam attenuation coefficient). Statistical model has been established to link profile of beam attenuation coefficient from profiles of temperature, salinity, and chlorophyll-*a* fluorescence.

Bioluminescence represents an operational threat to night time operations or additional capabilities in detecting and tracking surface and subsurface movement during the night. As submarines are getting quieter, this alternative mean of detection is prevalent in littoral zone where conventional acoustic surveillance is severely challenged. However, the source term (i.e., bioluminescence) is neglected in the existing Navy's EODES model. A simplified algorithm with source term in the RTE is presented and integrated with observed volume scattering coefficient for the East Asian Marginal Seas.

ACKNOWLEDGMENTS

This research was sponsored by OPNAV-N97 (topic sponsor: Dr. Andrew Greene) through NPS Naval Research program and ONR (program manager: Mr. Brian Almquist).

REFERENCES

[1] Farr, N., Freitag, L., and Jakuba, M., "Underwater acoustic/optical communications and data connectivity, available online at http://www.whoi.edu/page.do?pid=119416&&tid=3622&&cid=163149 (2013).

[2] Chu, P.C., Wells, S.K., Haeger, S.D., Szczechowski, C., and Carron, M.J., "Temporal and spatial scales of the Yellow Sea thermal variability," Journal of Geophysical Research, 102, 5655-5668 (1997).

[3] Chu, P.C., Fralick, C.R., Haeger, S.D., and Carron, M.J., "A parametric model for Yellow Sea thermal variability," Journal of Geophysical Research, 102, 10499-10508 (1997).

[4] Chu, P.C., Chen, Y.C., and Kuninaka, A., "Seasonal variability of the East China/Yellow Sea surface buoyancy flux and thermohaline structure," Advances in Atmospheric Sciences, 22, 1-20 (2005).

[5] Chu, P.C., Tseng, H.C., Chang, C.P., and Chen, J.M., "South China Sea warm pool detected from the Navy's Master Oceanographic Observational Data Set (MOODS)," Journal of Geophysical Research, 102, 15761-15771 (1997).

[6] Chu, P.C., Lu, S.H., and Chen, Y.C., "Evaluation of the Princeton Ocean Model using the South China Sea Monsoon Experiment (SCSMEX) data," Journal of Atmospheric and Oceanic Technology, 18, 1521-1539 (2001).

[7] Chu, P.C. and Hsieh, C. P., "Change of multifractal thermal characteristics in the western Philippine Sea upper layer during internal wave-soliton propagation," Journal of Oceanography, 63, 927-939 (2007).

[8] Widder, E. A., Frey, C. L., and Borne, L. J., " HIDEX Generation II: a new and improved instrument for measuring marine bioluminescence," MTS/IEEE OCEANS 2003 Proceedings, 4, 2214–2221 (2003).

[9] Widder, E. A, Frey, C. L., and Bowers, J., "Improved bioluminescence measurement instrument – A new high-intake defined excitation bathyphotometer developed for the U.S. Navy," Sea Technology, 46, 1015 (2005).

[10] Cullen, A. J., "Hydrographic and Optical Characteristics of Adriatic Sea," M.S. thesis, Dept. of Oceanography, Naval Postgraduate School, 301 pp (2016).

[11] Breshears, B.F., "Hydrographic and Optical characteristics of East Asian Marginal Seas," M.S. thesis, Dept. of Oceanography, Naval Postgraduate School, 301 pp (2016).

[12] Hammerer, R.F., "Environmental effects of underwater optical transmission in the Arabian Gulf and the Gulf of Oman," M.S. thesis, Dept. of Oceanography, Naval Postgraduate School, 81 pp. (2016).

[13] Phung, T.Q., "Analysis of bioluminescence and optical variability in the Arabian Gulf and Gulf of Oman for Naval applications," M.S. thesis, Dept. of Oceanography, Naval Postgraduate School, 301 pp. (2013).

[14] Eriksen, C. C., Osse, T. J., Light, R. D., Wen, T., Lehman, T. W., Sabin, P. L., Ballard, J. W., Chiodi, A. M., "Seaglider: a long-range autonomous underwater vehicle for oceanographic research." IEEE Journal of Oceanic Engineering, 26, 424-436 (2001).
[15] Wet Labs Inc., "Environmental Characterization Optics", available online at http://wetlabs.com/content/eco-sensor-suite 2017.
[16] Boss, E., Stramski, D., Bergmann, T., Pegau, W.S., Lewis, M. "Why should we measure the optical backscattering coefficient?" Oceanography, 17(2) 44-49 (2004).
[17] Martinez, R.P., "Bio-optical and hydrographic characteristics of the western Pacific Ocean for undersea warfare using seaglider data," M.S. thesis, Dept. of Oceanography, Naval Postgraduate School, 83 pp. (2014).
[18] Giddings, T.E., and Shirron, J.J., "Software Design Document for the EODES Electro-Optical Identification Performance Prediction Model Version-1," CDRL Sequence No. 1, METRON, Prepared for Naval Oceanographic Office, pp. 113 (2011).
[19] Mobley, C., "*Ocean Optics*," available at http://www.oceanopticsbook.info/view/introduction/overview (2016).
[20] Li, C., Park, K., Alouini, M.-S., "On the use of a direct radiative transfer equation solver for path loss calculation in underwater optical wireless channels," IEEE Wireless Communications Letters, doi: 10.1109/LWC.2015.2459697 (2015).